International Journal of Electric Power and Energy Studies
ISSN: 3006-2004 (Print), ISSN: 3006-0826 (Online) | Volume 5, Number 2, Year 2026
DOI: https://doi.org/10.62051/ijepes.v5n2.01
Journal homepage: https://wepub.org/index.php/IJEPES/index

Research on Parameter Design and Control Strategy of Bidirectional CLLC Resonant Converter

Huachen Ding[1, *], Jie Zhu[2], Haohui Yuan[3]

[1] College of Mechanical Engineering, University of Shanghai for Science and Technology, Shanghai, China

[2] College of Mechanical Engineering, University of Shanghai for Science and Technology, Shanghai, China

[3] College of Mechanical Engineering, University of Shanghai for Science and Technology, Shanghai, China

[*]Corresponding Author: Huachen Ding

ABSTRACT

Under the context of energy structure transition and rapid advancement in power electronics, DC-DC converters, as key interface circuits for efficient power conversion and stable power supply, have become core components in modern power systems. Among various DC-DC converter topologies, the CLLC resonant converter features high power density and excellent galvanic isolation. Its topology typically integrates a high-frequency transformer for energy transfer, which not only provides electrical isolation between input and output but also reduces the size of magnetic components by increasing the switching frequency, thereby enhancing system power density. However, parameter design of the CLLC resonant converter remains challenging, requiring a trade-off between gain flatness and soft-switching range in bidirectional operation, coordination of the complex coupling among multiple resonant elements and parasitic parameters, and satisfaction of frequency regulation and efficiency optimization under wide input/output voltage ranges-constraints that are numerous and mutually restrictive. During the control process, the system suffers from long settling time and slow dynamic response. To address these issues, this paper first introduces the topology of the CLLC resonant converter. In view of the difficulties in parameter design, the fundamental harmonic analysis (FHA) method is adopted to design the parameters of the CLLC resonant converter. Combined with the control strategy, a prototype design method for the CLLC converter is completed.

KEYWORDS

DC-DC Converter; CLLC Resonant Converter; Fundamental Harmonic Analysis; Design of Parameters; Soft-Switching; Closed-loop Control.

1. INTRODUCTION

With the rapid advancement of modern power electronics technologies, higher demands have been imposed on voltage level matching, efficient energy conversion, and stable power supply in various electrical energy systems. In this context, DC–DC converters, serving as critical power electronic devices for energy conversion between different DC voltage levels, play a pivotal role in fields such as renewable energy, electric vehicles, and information technology [1]–[3]. In renewable energy generation systems, such as photovoltaic power generation and energy storage systems, the output voltage typically varies with environmental conditions and operating states, whereas the load side or grid side requires a stable DC voltage. Therefore, DC–DC converters are required to perform both

step-up and step-down voltage regulation, while simultaneously enabling maximum power point tracking and energy management, so as to enhance the overall power generation efficiency and system stability. In the context of electric vehicles, multiple power systems with different voltage levels generally exist within the vehicle, such as the high-voltage traction battery bus, the motor drive system, and onboard electronic equipment [4]. The energy transfer among these different voltage levels relies on DC–DC converters for efficient conversion and regulation. Furthermore, in onboard chargers and energy storage systems, bidirectional power flow is required to accommodate both charging and discharging needs, which further underscores the importance of high-performance DC–DC converters [5].

In recent years, DC–DC converters have attracted extensive attention and research interest. The buck–boost converter is introduced in [6], offering flexibility in voltage regulation capability. However, in the conventional buck–boost topology, the power devices and the inductor current typically endure substantial current and voltage stresses. These stresses are further exacerbated under step-up or high-power conditions, thereby degrading system efficiency and increasing device losses. The Ćuk converter where energy transfer is accomplished via a capacitor, resulting in continuous input and output currents during operation. This characteristic endows the Ćuk converter with low current ripple. Nevertheless, since energy is transferred through a coupling capacitor, the circuit generally necessitates a large energy storage capacitor and two inductors, leading to a relatively complex circuit structure and increased physical volume. In certain applications, additional circuitry is required for polarity adjustment, further complicating system design. The SEPIC converter is discussed in [7], which is capable of maintaining a regulated output voltage by adjusting the duty cycle, regardless of whether the input voltage is higher or lower than the output voltage. This type of converter features a relatively intricate circuit structure, requiring two inductors and a coupling capacitor for energy transfer, which increases system volume and cost. The dual active bridge (DAB) converter is examined in [8], exhibiting excellent bidirectional power flow capability over a wide power range, while the high-frequency transformer provides galvanic isolation and enhances system power density. However, under light-load conditions, its soft-switching range is significantly reduced, leading to increased switching losses and consequently lower system efficiency. The LLC converter is reviewed in [9], which effectively reduces switching losses and improves system efficiency. Moreover, due to its high operating frequency, the size of magnetic components can be significantly minimized. Nevertheless, achieving bidirectional power transfer with the LLC topology proves challenging, thus imposing limitations in applications requiring bidirectional energy flow. The asymmetric CLLC converter is introduced in [10]–[12], which can reduce circulating current to some extent and improve power density. However, since the resonant parameters on the primary and secondary sides are no longer symmetrical, the voltage gain characteristics deteriorate noticeably during reverse power transfer, and the soft-switching range is narrowed, resulting in reduced efficiency under reverse operation.

The CLLC resonant converter investigated in this paper establishes symmetrical resonant networks on both the primary and secondary sides, enabling the circuit to maintain similar operating characteristics regardless of the power transfer direction. This topology exhibits favorable soft-switching properties, achieving zero-voltage switching (ZVS) for the primary-side switches and zero-current switching (ZCS) for the secondary-side devices over a wide load range. Consequently, switching losses are effectively reduced, and system efficiency is enhanced. Furthermore, owing to the symmetry of its resonant parameters, the CLLC converter enables highly efficient bidirectional power transfer, thereby offering significant advantages in on-board charging applications.

2. PARAMETER DESIGN BASED ON FHA MODELING

2.1. Operating Mode Analysis

Fig. 1 illustrates the topology of the symmetrical CLLC bidirectional DC–DC converter. The symmetric parameter configuration enables the converter to maintain similar resonant characteristics and voltage gain profiles during both forward and reverse power transfer. Owing to the symmetrical structure of the resonant network in both directions, the equivalent resonant parameters of the circuit remain substantially unchanged when the power transfer direction is reversed. Consequently, stable operation can be achieved without redesigning the control strategy or circuit parameters. This necessitates the satisfaction of the condition given in (1).

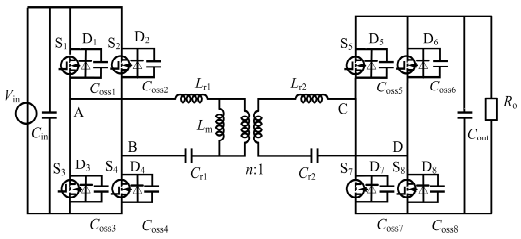

Fig. 1 Topology of the symmetric CLLC bidirectional DC-DC converter

$$\begin{cases} L_{r1} = n^2 L_{r2} \\ C_{r1} = \dfrac{C_{r2}}{n^2} \end{cases} \tag{1}$$

The operating modes of the CLLC resonant converter can be categorized into below-resonance mode, resonance mode, and above-resonance mode, with corresponding operating waveforms illustrated in Figs. 2, 3, and 4, respectively. Given that the positive and negative half-cycles of the CLLC converter are symmetrical, only the waveforms under forward operation are presented herein.

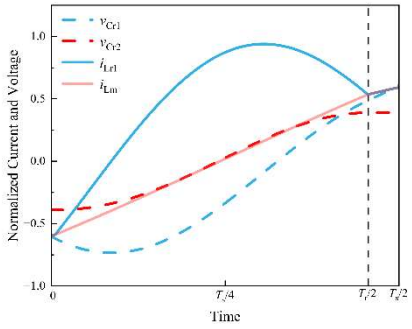

Fig. 2 Operation mode below resonance frequency (under-resonance mode)

In the below-resonance mode, where $f_r > f_s$, the primary-side currents i_{r1} and i_{Lm} exhibit identical initial values and become equal again prior to the end of the switching period, thereby enabling ZVS. Upon reaching the resonant cycle, the secondary-side devices turn off naturally, achieving ZCS.

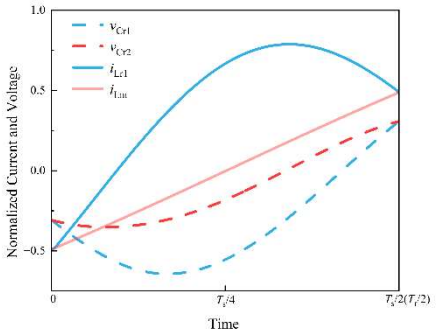

Fig.3 Quasi-resonance operation mode

In the resonance mode, where $f_r = f_s$, the resonant state can be regarded as a special case of the below-resonance mode. In this mode, i_{r1} and i_{Lm} are equal only at a single time instant rather than over an interval. The currents i_{r1} and i_{Lm} share the same initial value, undergo sinusoidal variation, and become equal again, thereby completing ZCS under the boundary condition.

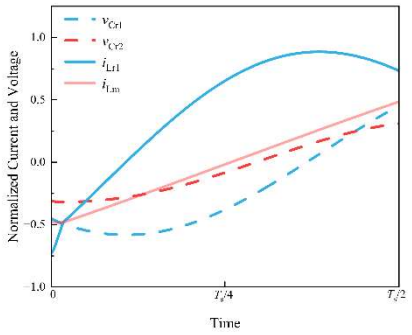

Fig. 4 Operation mode above resonance frequency (over-resonance mode)

In the above-resonance mode, where $f_r < f_s$, the switching period is shorter than the resonant period. Consequently, before the half-cycle of the resonant process is completed, the primary-side resonant current i_{r1} exceeds the magnetizing current i_{Lm}. The difference between these two currents flows through the primary winding of the transformer, resulting in a nonzero secondary-side resonant current.

From the foregoing operating mode analysis, it can be observed that in the above-resonance mode, the resonant current exceeds the magnetizing current and never decreases to the level of the magnetizing current. Consequently, ZCS cannot be achieved for the low-voltage side switches. In contrast, when the converter operates in the below-resonance or resonance mode, soft-switching can be realized, thereby enabling the converter to achieve high conversion efficiency.

2.2. Voltage Gain Analysis

Fig. 5 depicts the equivalent circuit of the CLLC resonant converter obtained through FHA. The quantities u_{AB} and u_{CD} represent the fundamental components of the voltages at ports AB and CD, respectively, as illustrated in Fig. 1. R_{eq} denotes the equivalent output resistance.

$$R_{eq} = \frac{8}{\pi^2} R_o \tag{2}$$

Based on the equivalent circuit shown in Fig. 6, the voltage gain of the CLLC resonant converter under FHA can be derived as

$$M = \frac{u_{CD}}{u_{AB}} = \frac{1}{\sqrt{(1+\frac{1}{k}-\frac{1}{kf_n^2})^2 + \frac{Q^2}{k^2}[(2k+1)f_n - \frac{2k+2}{f_n} + \frac{1}{f_n^3}]^2}} \tag{3}$$

In (3), M represents the voltage gain, $k = L_m/L_{r1}$ is the inductance ratio (magnetizing inductance to primary resonant inductance), and $f_n = f_s/f_r$ denotes the normalized frequency. The quality factor Q is expressed as

$$Q = \frac{Z_r}{R_{eq}} \tag{4}$$

In (4), $Z_r = \sqrt{L_r/C_r}$ denotes the characteristic impedance.

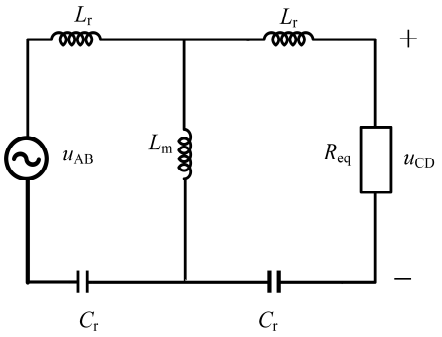

Fig. 5 Equivalent circuit of the CLLC resonant converter based on FHA

In high-frequency transformers, the magnetizing inductance is typically much larger than the resonant inductance. By setting the inductance ratio to $k = 10$, the relationship between the voltage gain M and the normalized frequency f_n can be plotted for different values of the quality factor Q. From the definition of Q, it follows that when the converter parameters are fixed, the quality factor is inversely proportional to the load. As can be observed in Fig. 6, at the resonant frequency, the voltage gain is unity ($M = 1$) regardless of the value of Q, i.e., independent of whether the load is heavy or light. As the quality factor increases, the voltage gain of the converter gradually decreases. Therefore, if the design objective is to maintain the voltage gain around unity, a relatively small value of Q should be selected.

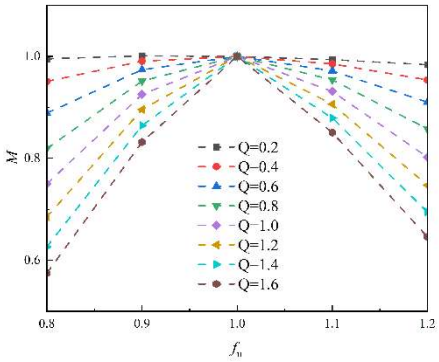

Fig. 6 Influence of quality factor on gain characteristics under the same inductance ratio

To evaluate the influence of the inductance ratio k on the voltage gain, the quality factor Q in (3) is set to 0.2, and the resulting gain curves for different values of k are obtained, as shown in Fig. 6.

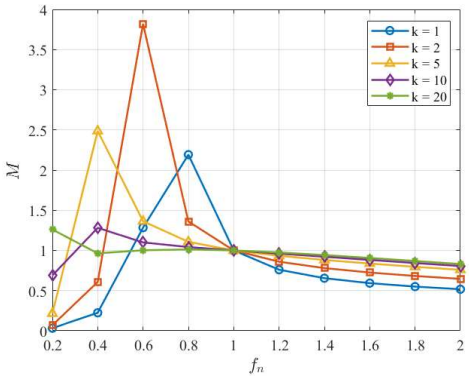

Fig. 7 Influence of inductance ratio on gain characteristics under the same quality factor

As can be observed in Fig.7, when the quality factor is fixed, the voltage gain characteristics of the CLLC resonant converter are primarily influenced by the inductance ratio k. In general, as the inductance ratio increases, the voltage gain curves become progressively flatter, while the frequency regulation range correspondingly decreases. Conversely, when the inductance ratio is relatively small, the coupling effect of the resonant network is enhanced, resulting in more pronounced peaks in the voltage gain curves near the resonant frequency and more drastic gain variations. Therefore, in practical design, a trade-off must typically be made between the gain regulation range and system stability, necessitating an appropriate selection of the inductance ratio[13].

$$t_{\mathrm{d}} \geq 8 f_{\mathrm{smax}} L_{\mathrm{m}} C_{\mathrm{oss}} \tag{5}$$

$$L_{\mathrm{m}} \leq \frac{t_{\mathrm{d}}}{8 f_{\mathrm{smax}} C_{\mathrm{oss(max)}}} \tag{6}$$

In the design process, since the dead time t_d is typically predetermined, it can be used to constrain the value of the magnetizing inductance. Setting the resonant frequency to 100 kHz, the dead time to 200 ns, and the maximum junction capacitance to 58 pF, substituting these values into (6) yields a maximum magnetizing inductance of 4.31 mH.

The foregoing analysis addresses conduction losses. However, transmission losses also constitute a significant factor affecting converter efficiency. Minimizing these losses during normal converter operation is therefore a key objective in the parameter design process. The currents on both sides of the high-frequency transformer are the primary determinants of transmission losses. The expressions for calculating the primary-side and secondary-side currents can be expressed as

$$\begin{cases} {i_{\mathrm{P\_rms}}}^2(t) = \dfrac{V_{\mathrm{o}}}{8}[(\dfrac{\pi}{R_{\mathrm{o}}})^2 + (\dfrac{T_{\mathrm{s}}}{2L_{\mathrm{m}}})^2] \\ {i_{\mathrm{S\_rms}}}^2(t) = \dfrac{V_{\mathrm{o}}^2}{16}[\dfrac{1}{{R_{\mathrm{o}}}^2} + (\dfrac{T_{\mathrm{s}}}{L_{\mathrm{m}}})^2(\dfrac{5\pi^2 - 48}{12\pi^2})] \end{cases} \tag{7}$$

From (7), it can be seen that increasing L_m effectively reduces the RMS current flowing through the transformer, thereby decreasing switching losses. However, as indicated by (6), L_m is subject to an upper limit imposed by design constraints. Therefore, in the design process, the inductance ratio k must be appropriately selected. Based on a comprehensive consideration of these factors, $k = 5$ was ultimately chosen, and the magnetizing inductance was finalized as $L_m = 112\,\mu_{\mathrm{H}}$. Consequently, the following parameters can be obtained:

$$L_{r1} = \frac{L_m}{k} \approx 22.4\mu\mathrm{H} \tag{8}$$

The turns ratio of the high-frequency transformer investigated in this paper is $n = 1.5$. Substituting this value into (1) yields the secondary-side resonant inductance

$$L_{r2} = \frac{L_{r1}}{n^2} \approx 9.96\mu\mathrm{H} \tag{9}$$

When the converter operates in the full-resonance mode, the resonant capacitance can be determined using the series resonance formula:

$$C_{\mathrm{r1}} = \frac{1}{(2\pi f_{\mathrm{r}})^2 L_{\mathrm{r1}}} \approx 113.08\mathrm{nF} \tag{10}$$

$$C_{\mathrm{r2}} = n^2 C_1 \approx 254.43\mathrm{nF} \tag{11}$$

3. RESEARCH ON CONTROL STRATEGIES FOR RESONANT CONVERTERS

3.1. Introduction to PI Control Strategy

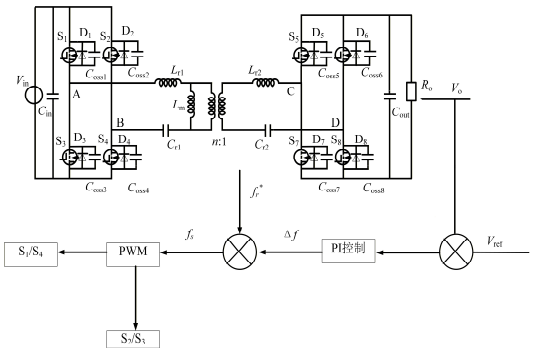

Fig. 8 Schematic diagram of the PI closed-loop control strategy

The PI control method achieves stable output voltage regulation by continuously sampling the output voltage, comparing it with a preset reference voltage, and adjusting the switching frequency based on the resulting error.

First, the system establishes a desired reference voltage V_{ref}, while the actual output voltage V_o is obtained through the sensing circuit. The voltage error is obtained by comparing these two values

$$e(t) = V_{\text{ref}} - V_{\text{o}} \tag{12}$$

This error signal is fed into the proportional–integral (PI) controller for regulation. The PI controller processes the error through its proportional and integral actions, and its output can be expressed as:

$$u_c(t) = K_{\text{p}} e(t) + K_{\text{i}} \int_0^t e(\tau) d\tau \tag{13}$$

Here, K_p represents the proportional gain, and K_i represents the integral gain. The function of the PI controller is to adjust the control variable based on the output voltage deviation, thereby endowing the system with favorable steady-state accuracy and dynamic response performance. Subsequently, the output signal of the PI controller serves as the input control variable for the voltage-controlled oscillator (VCO). The VCO generates an oscillating signal at a frequency corresponding to the magnitude of the input control voltage. The relationship between its output frequency and the control voltage is typically linear:

$$f_{\text{s}} = f_{\text{r}} + K_{\text{v}} u_c(t) \tag{14}$$

Here, f_s denotes the switching frequency, f_r repr(15)esents the resonant frequency, and K_v is the frequency modulation gain.

Finally, the frequency signal generated by the VCO is fed into the PWM module. Based on this frequency, the PWM module generates corresponding driving pulse signals to control the turn-on and turn-off of the full-bridge switches. As the switching frequency varies, the voltage gain of the resonant network changes accordingly, causing the output voltage to progressively approach the reference voltage. This process ultimately achieves closed-loop voltage regulation.

3.2. Overview of an Improved Control Strategy

The fundamental concept of the improved control strategy is to estimate the system states and external disturbances in real time using an observer, and subsequently compensate for them in the control law, thereby enhancing the dynamic performance and disturbance rejection capability of the system.

From the perspective of control theory, the voltage loop of the CLLC resonant converter can be regarded as the plant to be controlled, which can be simplified as a second-order system.

$$\begin{cases} \dot{x}_1 = x_2 \\ \dot{x}_2 = f + b_0 u \\ y = x_1 \end{cases} \tag{15}$$

Here, x_1 denotes the system output, x_2 represents the rate of change of the output, u is the control input, b_0 is the system input gain, f represents the total disturbance, and y denotes the actual system output.

To facilitate disturbance analysis, the total disturbance is augmented as a new state variable.

$$x_3 = f \tag{16}$$

Based on the augmented state variables, the linear extended state observer (LESO) is constructed as follows:

$$\begin{cases} \dot{z}_1 = z_2 + \beta_1 (y - z_1) \\ \dot{z}_2 = z_3 + \beta_2 (y - z_1) + b_0 u \\ \dot{z}_3 = \beta_3 (y - z_1) \end{cases} \tag{17}$$

Here, z_1 denotes the estimated output voltage, z_2 represents the estimated rate of change of the output voltage, and z_3 is the estimated total disturbance. The parameters β_1, β_2, and β_3 are the observer gains. These gains are typically determined using the bandwidth tuning method.

$$\begin{cases} \beta_1 = 3\omega_0 \\ \beta_2 = 3\omega_0^{\,2} \\ \beta_3 = \omega_0^{\,3} \end{cases} \tag{18}$$

Once the estimated system states and disturbance are obtained, the control law can be formulated as follows:

$$\begin{cases} u = \dfrac{u_0 - z_3}{b_0} \\ u_0 = k_p(V_{\text{ref}} - V_{\text{o}}) \end{cases} \tag{19}$$

By subtracting the estimated disturbance z_3 from the observer, feedforward compensation for the system disturbance is achieved. To ensure system stability and robustness, the controller bandwidth must be lower than the observer bandwidth. Typically, the observer bandwidth is designed to be three to five times the controller bandwidth. Consequently, the transfer function of the control input u can be obtained as follows:

$$u = \frac{G(s)}{b_0 M(s)} R(s) - \frac{Q(s)}{b_0 M(s)} Y(s) \tag{20}$$

$$\begin{cases} G(s) = k_d(s + \omega_0)^3 \\ Q(s) = \omega_0[s^2\omega_0^2 + 2\omega_c(\omega_0^2 + 3\omega_0 s \\ + 3s^2) + \omega_0\omega_c^2(3s^2 + \omega_0 s)] \\ M(s) = (1 + \omega_c^2)(s + \omega_0)^3 + \\ \omega_c(2s^3 - 3s^2\omega_0^2 - s\omega_0^3) + (\omega_0^3 - s^2\omega_0^3) \end{cases} \tag{21}$$

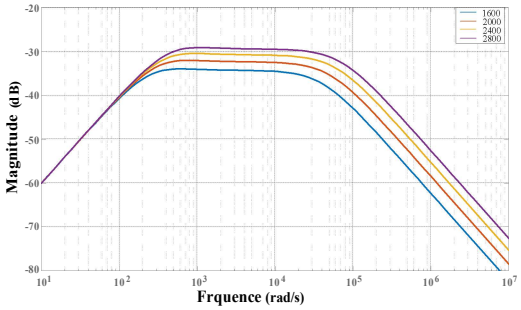

Fig. 9 Transfer Block Diagram

It can be observed from the transfer block diagram that the control input experiences a gain with respect to the output-side disturbance. This gain is typically influenced by the control gain, controller bandwidth, and observer bandwidth. At the target frequency, as the bandwidth increases, the disturbance signal does not compromise the stability margin.

4. EXPERIMENTAL VALIDATION

Since the CLLC resonant converter features bidirectional power flow with symmetrical forward and reverse characteristics, only its forward operation is validated herein. As can be observed from the waveforms in Fig. 9, under the preset input/output voltage targets and with an appropriate dead time setting, the parasitic capacitances of the switching devices complete the charging and discharging

process within a very short interval. This ensures that during the dead time, the parasitic capacitances are fully charged/discharged, enabling zero-voltage switching (ZVS) for all primary-side switches. Subsequently, when switches S_1 and S_4 remain in the on-state, the primary-side resonant current equals the magnetizing current, resulting in zero secondary-side resonant current. Consequently, the body diodes of secondary-side switches$S_5$and S_8 turn off naturally as i_2 gradually decreases to zero, thereby achieving zero-current switching (ZCS) without the reverse recovery issue associated with the body diodes.

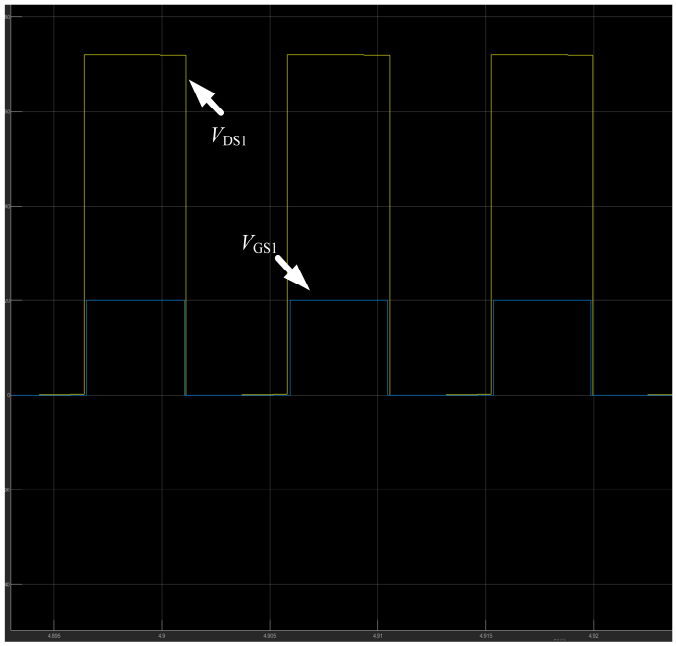

Fig. 10 Simulation Diagram

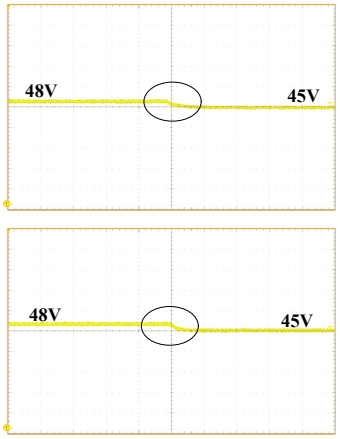

Fig. 11 illustrates the transient process when the output voltage steps down from 48 V to 45 V

The PI controller exhibits a relatively sluggish response, characterized by the longest settling time and no overshoot. In contrast, the improved control strategy demonstrates significantly better dynamic performance-also with no overshoot, but with a shorter settling time. This improvement is primarily attributed to the fact that the improved control strategy treats parameter uncertainties, load variations, and harmonic components collectively as a total disturbance, which is estimated in real time and compensated for in the control law. Consequently, it mitigates the impact of harmonic disturbances on the dynamic performance of the system to a certain extent.

5. SUMMARY

In this paper, an equivalent model of the CLLC resonant converter was established based on fundamental harmonic approximation (FHA). The relationship between voltage gain and normalized frequency under different values of Q and k was analyzed, providing a theoretical foundation for the design of resonant parameters. Key system parameters were designed by considering the application requirements and loss model of the CLLC bidirectional full-bridge DC–DC converter. To achieve output voltage regulation, an improved control strategy was proposed and compared with the conventional PI controller, demonstrating superior dynamic response capability. Finally, an experimental prototype was constructed for validation. The experimental results indicate that the proposed design methodology enables the CLLC converter to not only achieve ZVS operation but also significantly reduce output voltage ripple, while exhibiting enhanced dynamic performance during transient processes.

REFERENCES

[1] C. Zhang, J. Gu, X. Zhu, L. Xu, Y. Du and H. Zheng, "A Common Ground Series–Parallel Switched-Inductors Bidirectional DC–DC Converter With Wide Voltage Gain and Zero Input Current Ripple," in IEEE Transactions on Industrial Electronics, vol. 72, no. 8, pp. 7672-7682, Aug.2025.

[2] A. Chandwani and A. Mallik, "Parasitic Component Small-Signal Modeling and Control of a Practical CLLC Resonant Converter," in IEEE Journal of Emerging and Selected Topics in Power Electronics, vol. 11, no. 2, pp. 1477-1495, April 2023.

[3] Y. Wang et al. , “A multiple modular isolated DC/DC converter with bidirectional fault handling and efficient energy conversion for DC distribution network,” IEEE Trans. Power Electron., vol. 35, no. 11, pp. 11502-11517, Nov. 2020.

[4] Y. Wang et al., “A Dual-Active-Bridge with Half-Bridge submodules DC Solid-State transformer for DC distribution networks,” IEEE Journal of Emerging and Selected Topics in Power Electron., vol. 9, no. 2, pp. 1891-1904, Apr. 2021.

[5] Z. Yao, X. He, M. Liu, J. Liu, Z. Xiao and Y. Tang, "Fixed Switching Frequency Control Using Trapezoidal Current Mode to Achieve ZVS in Three-Level DC–DC Converters," IEEE Transactions on Industrial Electronics, vol. 72, no. 4, pp. 4175-4185, April 2025.

[6] J. Liao, G. Qiu, Y. Huang and V. Khadkikar, "Lagrange-Multiplier-Based Control Method to Optimize Efficiency for Four-Switch Buck–Boost Converter Over Whole Operating Range," IEEE Trans. Ind. Electron., vol. 71, no. 1, pp. 822-833, Jan. 2023.

[7] Z. Yan, J. Zeng, Z. Guo, R. Hu and J. Liu, "A Soft-Switching Bidirectional DC–DC Converter With High Voltage Gain and Low Voltage Stress for Energy Storage Systems," IEEE Trans. Ind. Electron., vol. 68, no. 8, pp. 6871-6880, Aug. 2021.

[8] N. Wang, Y. Jiang, W. Hu, Y. Wang and Z. Chen, "An ANN-Aided Parameter Design Method for CLLC-Type DAB Converters Considering Parameter Perturbation," in IEEE Transactions on Industrial Electronics, vol. 72, no. 4, pp. 3735-3745, April 2025.

[9] C. Ma, X. Zhu, Z. Chen and B. Zhang, "Time Domain Analysis and Gain Curve Modeling of Fractional-Order Full-Bridge LLC Resonant Converter," in IEEE Transactions on Power Electronics, vol. 40, no. 9, pp. 13035-13049, Sept. 2025.

[10] R. He et al., "Resonant Frequency Tracking Scheme for LLC Converter Based on Large and Small Signal Combined Model," in IEEE Access, vol. 11, pp. 83390-83399, Jul 2023.

[11] G. Ghosh, S. Vyapari and V. N. R, "Extended Phasor Analysis-Based Unified Approach to Accurate Small-Signal Modeling of LLC Resonant Converters," in IEEE Transactions on Power Electronics, vol. 40, no. 9, pp. 12906-12919,Sept.2025.

[12] L. Zhu, Z. Sheng, F. Peng and L. Yang, "Control Strategy of Half-Bridge Three-Level LLC Resonant Converters With Wide Output Voltage Range," in IEEE Transactions on Plasma Science, vol. 50, no. 11, pp. 4381-4386, Nov. 2022.

[13] J.-H. Jung, H.-S. Kim, M.-H.Ryu, and J.-W.Baek, “Design methodology of bidirectional CLLC resonant converter for high-frequency isolation of DC distribution systems,” IEEE Trans. Power Electron., vol. 28, no. 4, pp. 1741-1755, April. 2013.